nature geoscience

LETTERS

PUBLISHED ONLINE: 2 OCTOBER 2011 | DOI: 10.1038/NGEO1266

A model for orbital pacing of methane hydrate destabilization during the Palaeogene

Daniel J. Lunt[1]*, Andy Ridgwell[1], Appy Sluijs[2], James Zachos[3], Stephen Hunter[4] and Alan Haywood[4]

A series of transient global warming events[1,2] occurred during the late Palaeocene and early Eocene, about 59 to 50 million years ago. The events, although variable in magnitude, were apparently paced by orbital cycles[2–4] and linked to massive perturbations of the global carbon cycle[5,6]. However, a causal link between orbital changes in insolation and the carbon cycle has yet to be established for this time period. Here we present a series of coupled climate model simulations that demonstrate that orbitally induced changes in ocean circulation and intermediate water temperature can trigger the destabilization of methane hydrates. We then use a simple threshold model to show that progressive global warming over millions of years, in combination with the increasing tendency of the ocean to remain in a more stagnant state, can explain the decreasing magnitude and increasing frequency of hyperthermal events throughout the early Eocene. Our work shows that nonlinear interactions between climate and the carbon cycle can modulate the effect of orbital variations, in this case producing transient global warming events with varying timing and magnitude.

From the late Palaeocene to the early Eocene (~59–50 Myr), Earth's surface and oceans went through an interval of progressive warming, culminating in the early Eocene climatic optimum (EECO, ~51 Myr; ref. 6; Fig. 1). Superimposed on this gradual warming trend are a series of 'hyperthermal' events—geologically abrupt (<10 kyr) warmings of Earth's surface and deep ocean, the most prominent of which being the Palaeocene–Eocene Thermal Maximum (PETM, ~56 Myr; ref. 6). Two subsequent smaller events, ETM2 (~54 Myr; ref. 2), and ETM3 (~53 Myr; ref. 7) seem to share similar characteristics. Associated with the hyperthermals are large negative carbon-isotope excursions of surficial carbon reservoirs and dissolution of deep-sea carbonate (Fig. 1; refs. 8), consistent with massive injections of ^{13}C-depleted carbon into the ocean–atmosphere system. Proposed sources for this carbon include methane hydrates[5], terrestrial peat deposits[9], and thermogenic methane[10]. Understanding the causes of hyperthermals is important, not least because the amount of the carbon release and magnitude of global warming can be used to estimate climate sensitivity. The hyperthermals also reflect possible threshold events ('tipping points'), with slow changes in boundary conditions giving rise to rapid positive feedback and state transitions in the carbon–climate system[11–13].

Cyclostratigraphic evidence from complete marine sections suggest that the PETM, ETM2, and ETM3 events all initiated on maxima in the 100 kyr eccentricity cycle[2–4]. This has led to the suggestion that orbital pacing controlled the timing of carbon injection[2,4] and hence the occurrence of the hyperthermal events.

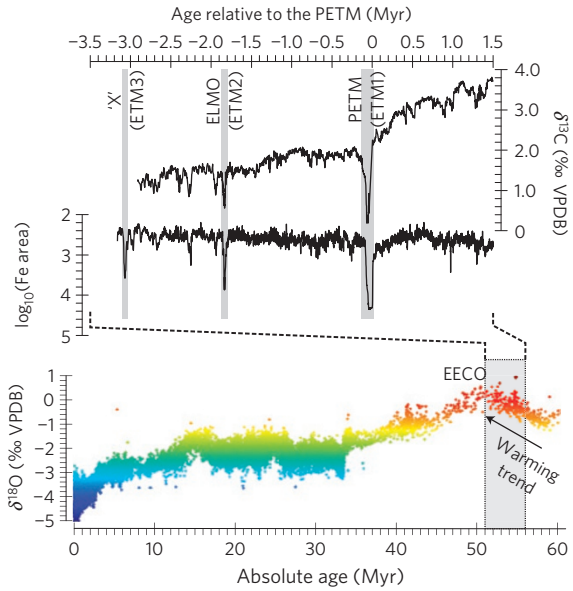

Figure 1 | Climatic context to the Palaeogene hyperthermal events. Shown at the top are the three major hyperthermal events during the early Eocene—PETM (ETM1), ELMO (ETM2), and X (ETM3) events, as recorded in benthic carbon isotopic ($\delta^{13}C$) and core XRF scans of iron content (Fe area)[8]. These are plotted on a floating orbitally tuned timescale relative to the onset of the PETM (ref. 8). The bottom plot shows the benthic $\delta^{18}O$ stack of Zachos *et al.*[1] against absolute age, to illustrate the climatic context in which the major hyperthermal events occur—that is, a period of progressive warming starting at ~59 Myr and culminating in the EECO, (~52–50 Myr).

However, no published explanation exists of how a strong imprint of orbital cycles on early Palaeogene terrestrial[14], shallow[15], or deep marine sediments[3,16] can arise, particularly in light of the absence of large ice-sheets in the Eocene system, which play a crucial role in amplifying orbital-scale climatic fluctuations in the Quaternary.

To investigate the role of orbital variations, we have carried out a suite of fully coupled atmosphere–ocean climate general circulation model (GCM) simulations under Eocene boundary conditions, testing permutations of two background levels of atmospheric carbon dioxide concentration and four orbital configurations. The 'low' and 'high' carbon dioxide (CO_2) concentrations are 560 (×2 pre-industrial) and 1,120 (×4 pre-industrial) parts per million by volume (ppmv), respectively, and hence span current uncertainty in proxy estimates of atmospheric CO_2 at this time[1]. The four assumed

[1]School of Geographical Sciences, University of Bristol, University Road, Bristol BS8 1SS, UK, [2]Biomarine Sciences, Institute of Environmental Biology, Utrecht University, Laboratory of Palaeobotany and Palynology, Budapestlaan 4, 3584 CD Utrecht, The Netherlands, [3]Earth and Planetary Sciences, University of California, Santa Cruz, California 95064, USA, [4]School of Earth and Environment, University of Leeds, Leeds LS2 9JT, UK.
*e-mail: d.j.lunt@bristol.ac.uk.

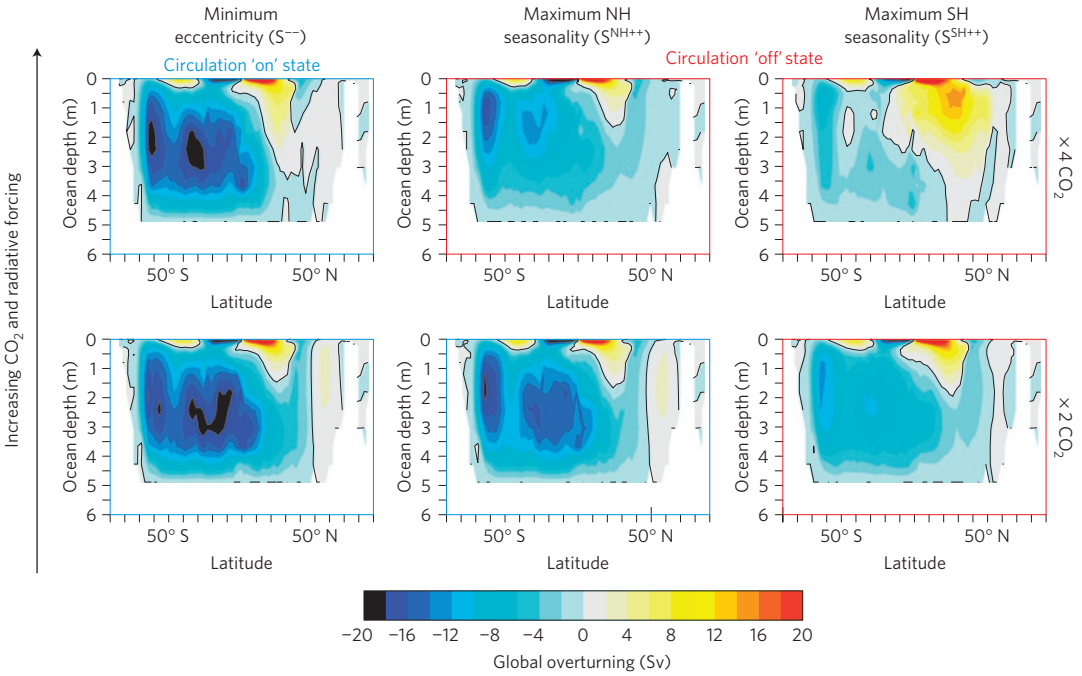

Figure 2 | Orbital and greenhouse modulation of the Palaeogene ocean circulation switch. Shown are the model-predicted global overturning circulation state under two different atmospheric pCO_2 forcings (×2 and ×4 CO_2 going up the *y* axis) versus three different idealized orbital configurations—minimum eccentricity, maximum seasonality in the Northern Hemisphere, and maximum seasonality in the Southern Hemisphere (non-dimensional along the *x* axis). Global ocean circulation states in which the southern source is weak - the 'off' state, are highlighted with a red border (and the 'on' state in blue).

orbital configurations create conditions representing: minimum eccentricity (S^{--}), maximum Northern Hemisphere and Southern Hemisphere seasonality (S^{NH++} and S^{SH++}, respectively), and modern as a point of comparison. (See Methods and Supplementary Information for a full description of the simulations, including model boundary conditions and model-data comparison.)

At low (×2) CO_2, we find that a shift from the S^{--} to the S^{SH++} orbital configuration drives a significant reduction in deep water formation in the Southern Ocean (Fig. 2). This response is qualitatively similar to the effect found in two recent Eocene model studies that demonstrated an ocean circulation change characterized by anomalous warming patterns of intermediate waters induced by increased greenhouse gas concentrations[17,18]. Changing ocean circulation at the PETM is also supported by data from deep sea sediments, in particular interbasinal variations in $CaCO_3$ dissolution[19] and sediment bioturbation[20]. The circulation switch caused by the transition from S^{--} to S^{SH++} orbit is associated with a decrease in deep water formation off the Antarctic coast in the Pacific sector of the Southern Ocean (Supplementary Fig. S1) and a local freshening of the surface ocean water masses, which, in turn, is consistent with an increase in the local surface water budget (Supplementary Fig. S2). Critically, a significant warming at 800–1,200 m in the model (Supplementary Fig. S3) is also induced, with maximum warming (>2.5 °C) in the northern Indonesian seaway and in the southern Indian Ocean. As intermediate depths have been postulated to be critical to methane hydrate stability in the Palaeogene[21], we hence provide a mechanistically plausible link between sedimentary carbon inventory and orbital changes. We further find that the impact of orbital variations is a function of the background climate. For instance, at high (×4) CO_2, ocean circulation is in the 'off' state with S^{SH++} and S^{NH++} orbits, but is in the 'on' state with the S^{--} orbit (Fig. 2). Hence, orbital changes have the potential to trigger reorganizations of ocean circulation, but with a threshold dependent on the state of background (CO_2-driven) warming.

We find further support for this link between orbitally driven warming and hydrate destabilization by calculating the change in depth of the hydrate stability zone (HSZ), given a transient climate change from S^{--} to S^{SH++} and back to S^{--} on precessional timescales (Fig. 3; details of the calculation are given in Supplementary Information). The change in temperature induces a decrease in the depth of the stability zone in many coastal regions of the globe. In particular, large changes are seen north of Australia, on the eastern coasts of Eurasia, Africa and North America, and in the Tethys and para-Tethys seas. The many uncertainties involved (such as sedimentation rates, available organic carbon at the seafloor, and sedimentary diagenesis) make a calculation of the total inventory of hydrate release highly problematic, but our calculation does indicate that the sources could potentially be widespread.

The implied coupling between orbital forcing, ocean circulation, intermediate warming, hydrate inventory and global climate can be represented using a simple threshold model, similar to those developed to simulate Quaternary glaciations[22]. Our threshold model (see Supplementary Information) assumes a steady background CO_2 forcing, imprinted with orbital variations (Fig. 4a). The intermediate ocean (Fig. 4b) responds linearly to the background forcing, but warms rapidly once a threshold in the total forcing is exceeded, associated with an ocean switch in circulation as predicted in our GCM simulations. The submarine hydrate store responds linearly to the intermediate ocean temperature, but once depleted recharges on timescales of ~500,000 years (Fig. 4c). The global mean temperature (Fig. 4d) is simply assumed proportional to the background climate forcing plus released methane hydrate, which is decayed on a timescale of ~20,000 years.

The largest event predicted in our threshold model (EVENT1, analogous with the PETM, Fig. 4d) is consistent with the first occurrence of a switch in circulation and a substantial depletion of the methane hydrate reservoir. As CO_2 is still relatively low, circulation switches back to the 'on' state easily as the orbital forcing wanes, and the event is followed by hydrate recharge (Fig. 4c). With progressive background warming, the next orbital triggering

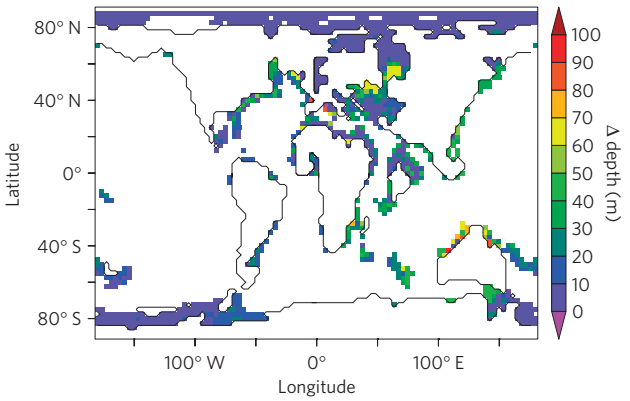

Figure 3 | Maximum decrease in depth of the HSZ, given a transient orbitally driven temperature forcing. The temperature forcing is from simulation S^{--} to S^{SH++} and back to S^{--} on a precessional timescale (details are given in Supplementary Section S4). Only near-coastal changes are plotted (where the ocean floor <2,500 m deep).

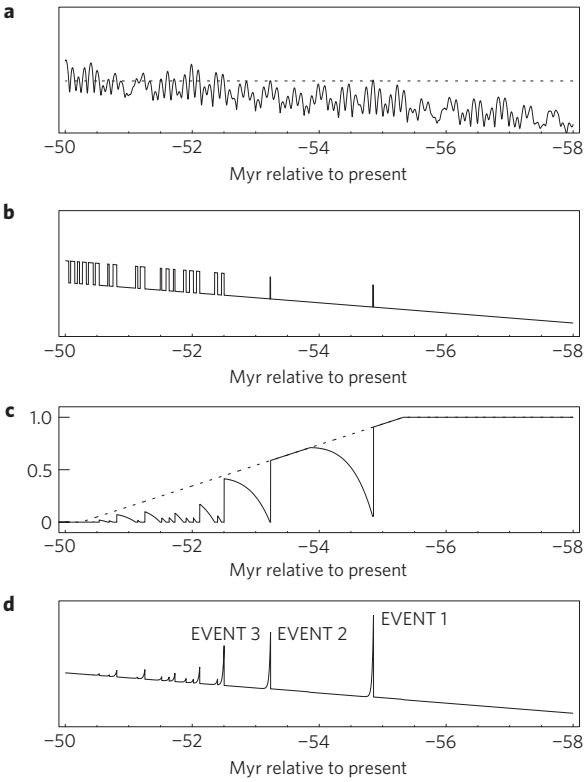

Figure 4 | Pacing of methane hydrate destabilization during the Palaeogene from our threshold model. The model is forced by gradual CO_2 forcing imprinted with orbital variations from 58 to 50 Myr. **a**, Forcing (dotted line shows the threshold for the ocean circulation switch). **b**, Response of the intermediate ocean temperature. **c**, Hydrate storage (dotted line shows the potential hydrate storage in the absence of orbital variations). **d**, Global mean temperature response. For comparison with Supplementary Figs S4–S7, which show the behaviour of the model under modified orbital forcing, comparison with proxy data, and the impacts of varying various tunable parameters.

is easier (EVENT2, an ETM2-like event, Fig. 4d). However, at this time there is also a decreased potential submarine hydrate store, meaning that the EVENT2 hyperthermal is smaller in magnitude. Critically, as ocean switches occur increasingly readily in a warmer world, the third (ETM3-like) and subsequent events occur after shorter intervals. Finally, at very high background CO_2, hydrates become unimportant as the potential hydrate storage approaches zero. Hence, our theory provides not only a physical mechanism for carbon injection during the hyperthermals but also for decreasing magnitude and increasing frequency during the Early Eocene. Furthermore, the occurrence of several double events in the geological record separated by 100 kyr (refs 8,23,24) is also predicted by this threshold model (Fig. 4d); such events would be unlikely to occur if a purely stochastic forcing were applied. The smaller magnitude of the second event is due to the depletion of the hydrate store in the first event, followed by insufficient time to recharge.

The orbital forcing we have applied in the threshold model is simply the eccentricity component of the Laskar solution from 58 to 50 Myr. In reality it is likely that the triggering also depends on the precessional and obliquity components; therefore, our threshold model is not designed to be predictive of the exact timing, pacing or magnitude of Palaeogene hyperthermals (see Supplementary Fig. S4). However, the qualitative results of the model, including decreasing strength and increasing frequency, and the existence of 'paired' events, are robust, and independent of the period of orbital forcing applied (see Supplementary Fig. S5). Moreover, by tuning certain parameters within the conceptual model, such as the threshold at which the circulation switch occurs, and by using alternative age models for the data (for example shifting the age of the PETM within the dating uncertainties), it is possible to obtain good agreement between the conceptual model and the data, including the timing of both pre- and post-PETM hyperthermals (see Supplementary Figs S6–S7). However, such agreement should be treated with extreme caution, given the many degrees of freedom in both the conceptual model and age model. The real world behaviour is much more complex than predicted by the threshold model, not least because, although our GCM simulations point towards the existence of a transition from strong to weak overturning, given the complexity of the forcing associated with orbital variations it is likely that response of the ocean circulation, and hence temperatures and hydrate state, is also extremely complex. Furthermore, it is important to note that following hydrate release and associated warming, other carbon cycle–climate feedbacks (not included in the threshold model) could become important, possibly resulting in multiple sources of ^{13}C-depleted carbon associated with the hyperthermals. Furthermore, the precise timing of events could be primed by non-orbital forcing, such as enhanced volcanic carbon emissions, potentially enhancing the sensitivity of the system to orbital forcing; this is particularly true for the largest event, the PETM, which seems to occur during a minimum in the 400-yr eccentricity cycle[3,25]. However, the conceptual model is actually rather generic, and similar or identical equations could equally be used to represent other hypotheses for orbital pacing of hyperthermals, for example the release of oceanic dissolved organic carbon[26].

Our coupled climate modelling demonstrates how orbital forcing superimposed on a long-term climate trend can provide a physically based mechanism for submarine methane hydrate destabilization, related to switches in ocean circulation and resulting warming at ocean intermediate depths. We can also conceptually explain both the decreasing magnitude and increasing frequency of hyperthermals through long-term Early Eocene warming, and the existence of paired events. Although we cannot robustly constrain the precise timing of the triggering threshold for the hyperthermals in terms of a specific set of climate or orbital conditions, our work implies that progressive changes in background climatic state significantly influences the timing and magnitude of past climate shifts that are paced by orbital forcing, and has close parallels with efforts towards understanding the late Neogene glacial–interglacial cycles[22,27].

Methods

We carried out eight simulations with the UK Met Office GCM, HadCM3L (ref. 28), with the MOSES2.2 land surface scheme. HadCM3L has a horizontal resolution in the atmosphere and ocean of 3.75° longitude by 2.5° latitude, with 19 vertical levels in the atmosphere and 20 in the ocean. This particular configuration of the model has been used and described previously[17]. The eight model simulations constitute all permutations of two different atmospheric CO_2 concentrations (low and high, ×2 and ×4 preindustrial, 560 and 1,120 ppm respectively) and four different orbital configurations modern, minimum eccentricity (S^{--}: eccentricity = 0.0, obliquity = 0.384 rad), high northern hemisphere seasonality (S^{NH++}: eccentricity = 0.054, obliquity = 0.428 rad, perihelion during boreal summer), and high southern hemisphere seasonality (S^{SH++}: eccentricity = 0.054, obliquity = 0.428 rad, perihelion during austral summer). The eight simulations are all 1,000 years in length (see Supplementary Fig. S8). The simulations at low and high CO_2 are continuations of the $2 \times CO_2$ and $4 \times CO_2$ simulations respectively presented in ref. 17, which are themselves more than 3,400 years in length. All simulations are carried out under Eocene boundary conditions (land–sea configuration, orography, and bathymetry, see Supplementary Fig. S9), and include a 0.4% decrease in solar constant relative to modern. The modelled sea surface temperature from the modern-orbit simulations are compared against background Eocene and PETM proxy temperature estimates[29] in Supplementary Fig. S10. With the exception of TEX86-derived estimates of extreme warmth in the Arctic ocean[30], the proxy sea surface temperature estimates from before and during the PETM event are broadly consistent with those of the $2 \times CO_2$ and $4 \times CO_2$ simulations respectively.

A full description of the threshold model, a comparison with Fe-count and $\delta^{13}C$ data, a series of sensitivity studies to model parameters, and a justification for the hydrate recharge time, is given in the Supplementary Information. A copy of the threshold model code itself is included in the Supplementary Information.

A description of the HSZ calculation is given in the Supplementary Information.

Received 4 July 2011; accepted 19 August 2011; published online 2 October 2011

References

1. Zachos, J. C., Dickens, G. R. & Zeebe, R. E. An early Cenozoic perspective on greenhouse warming and carbon-cycle dynamics. *Nature* **451,** 279–283 (2008).
2. Lourens, L. J. *et al.* Astronomical pacing of late Palaeocene to early Eocene global warming events. *Nature* **435,** 1083–1087 (2005).
3. Westerhold, T. *et al.* On the duration of magnetochrons C24r and C25n and the timing of early Eocene global warming events: Implications from the Ocean Drilling Program Leg 208 Walvis Ridge depth transect. *Paleoceanography* **22,** PA2201 (2007).
4. Galeotti, S. *et al.* Orbital chronology of Early Eocene hyperthermals from the Contessa Road section, central Italy. *Earth Planet. Sci. Lett.* **290,** 192–200 (2010).
5. Dickens, G. R., O'Neill, J. R., Rea, D. K. & Owen, R. M. Dissociation of oceanic methane hydrate as a cause of the carbon isotope excursion at the end of the Paleocene. *Paleoceanography* **10,** 965–971 (2005).
6. Zachos, J. C. *et al.* Rapid acidification of the ocean during the Paleocene–Eocene thermal maximum. *Science* **308,** 1611–1615 (2005).
7. Agnini, C. *et al.* An early Eocene carbon cycle perturbation at ~52.5 Ma in the southern Alps: Chronology and biotic response. *Paleoceanography* **24,** PA2209 (2009).
8. Zachos, J. C., McCarren, H., Murphy, B., Rohl, U. & Westerhold, T. Tempo and scale of late Paleocene and early Eocene carbon isotope cycles: Implications for the origin of hyperthermals. *Earth Planet. Sci. Lett.* **299,** 242–249 (2010).
9. Kurtz, A., Kump, L., Arthur, M., Zachos, J. & Paytan, A. Early Cenozoic decoupling of the global carbon and sulfur cycles. *Paleoceanography* **18,** 1090 (2003).
10. Svensen, H. *et al.* Release of methane from a volcanic basin as a mechanism for initial Eocene global warming. *Nature* **429,** 542–545 (2004).
11. Zachos, J. C., Lohmann, K. C. & Walker, J. C. G. Abrupt climate change and transient climates during the Paleogene—a marine perspective. *J. Geol.* **101,** 191–213 (1993).
12. Dickens, G. R., Castillo, M. M. & Walker, J. C. G. A blast of gas in the latest Paleocene: Simulating first-order effects of massive dissociation of oceanic methane hydrate. *Geology* **25,** 259–262 (1997).
13. Sluijs, A., Brinkhuis, H. & Schouten, S. Environmental precursors to rapid light carbon injection at the Palaeocene/Eocene boundary. *Nature* **450,** 1218–1221 (2007).
14. Abdul-Aziz, H. *et al.* Astronomical climate control on paleosol stacking patterns in the upper Paleocene-lower Eocene Willwood formation, Bighorn Basin, Wyoming. *Geology* **36,** 531–534 (2008).
15. Sluijs, A. *et al.* Paleocene-early Eocene paleoenvironments with special emphasis on the Paleocene–Eocene thermal maximum (Lomonosov Ridge, Integrated Ocean Drilling Program Expedition 302). *Paleoceanography* **23,** PA1S11 (2008).
16. Rohl, U., Norris, R. D. & Ogg, J. G. *Causes and Consequences of Globally Warm Climates in the Early Paleogene* Vol. 369 (Geological Society of America Special Paper, 2003).
17. Lunt, D. J. *et al.* CO_2-driven ocean circulation changes as an amplifier of Paleocene–Eocene thermal maximum hydrate destabilization. *Geology* **38,** 875–878 (2010).
18. Winguth, A., Shellito, C., Shields, C. & Winguth, C. Climate response at the Paleocene–Eocene thermal maximum to greenhouse gas forcing—a model study with CCSM3. *J. Clim.* **23,** 2562–2584 (2010).
19. Zeebe, R. E. & Zachos, J. C. Reversed deep-sea carbonate ion basin gradient during Paleocene–Eocene thermal maximum. *Paleoceanography* **22,** PA3201 (2007).
20. Panchuk, K., Ridgwell, A. & Kump, L. R. Sedimentary response to Paleocene–Eocene thermal maximum carbon release: A model-data comparison. *Geology* **36,** 315–318 (2008).
21. Dickens, G. R. Rethinking the global carbon cycle with a large, dynamic and microbially mediated gas hydrate capacitor. *Earth Planet. Sci. Lett.* **213,** 169–183 (2003).
22. Paillard, D. The timing of Pleistocene glaciations from a simple multiple-state climate model. *Nature* **391,** 378–381 (1998).
23. Cramer, B. S., Wright, J. D., Kent, D. V. & Aubry, M-P. Orbital climate forcing of $\delta^{13}C$ excursions in the late Paleocene–early Eocene (chrons C24n–C25n). *Paleoceanography* **18,** 1097 (2003).
24. Nicolo, M. J., Dickens, G. R., Hollis, C. J. & Zachos, J. C. Multiple early Eocene hyperthermals: Their sedimentary expression on the New Zealand continental margin and in the deep sea. *Geology* **35,** 699–702 (2007).
25. Charles, A. J. *et al.* Constraints on the numerical age of the Paleocene–Eocene boundary. *Geochem. Geophys. Geosyst.* **12,** Q0AA17 (2011).
26. Sexton, P. F. *et al.* Eocene global warming events driven by ventilation of oceanic dissolved organic carbon. *Nature* **471,** 349–352 (2011).
27. Raymo, M. E. The timing of major climate terminations. *Paleoceanography* **12,** 577–585 (1997).
28. Cox, P. M., Betts, R. A., Jones, C. D., Spall, S. A. & Totterdell, I. J. in *Meteorology at the Millennium* (ed. Pearce, R.) 259–279 (Academic, 2001).
29. Dunkley-Jones, T. *et al.* A Paleogene persepctive on climate sensitivity and methane hydrate instability. *Phil. Trans. R. Soc. A* **368,** 2395–2415 (2010).
30. Sluijs, A. *et al.* Subtropical Arctic Ocean temperatures during the Palaeocene/Eocene thermal maximum. *Nature* **441,** 610–613 (2006).

Acknowledgements

D.J.L. and A.R. acknowledge support from the UK Natural Environment Research Council grant NE/F001622/1. A.R. acknowledges support from The Royal Society in the form of a University Research Fellowship as well as NE/F002408/1 and NE/I006443/1. A.S. acknowledges support from the Netherlands Organisation for Scientific Research (NWO-Veni grant 863.07.001) and the research leading to these results has received funding from the European Research Council under the European Community's Seventh Framework Programme (FP7/2007-2013) / ERC Grant agreement 259627, awarded to A.S. This work was supported by NSF Grant OCE-0903014 to J.Z. S.H. acknowledges support from the UK Natural Environment Research Council grant NE/F021941/1.

Author contributions

D.J.L. and A.R. conceived the GCM model experiments and the threshold model; S.H. carried out the calculation of HSZ and the transient hydrate modelling. All authors interpreted and discussed the results and wrote the paper.

Additional information

The authors declare no competing financial interests. Supplementary information accompanies this paper on www.nature.com/naturegeoscience. Reprints and permissions information is available online at http://www.nature.com/reprints. Correspondence and requests for materials should be addressed to D.J.L.